Friction experiments on the nanometre scale

2001 J. Phys.: Condens. Matter 13 R619

(http://iopscience.iop.org/0953-8984/13/31/202)

INSTITUTE OF PHYSICS PUBLISHING JOURNAL OF PHYSICS: CONDENSED MATTER

J. Phys.: Condens. Matter **13** (2001) R619–R642 PII: S0953-8984(01)97992-5

TOPICAL REVIEW

Friction experiments on the nanometre scale

E Gnecco, R Bennewitz, T Gyalog and E Meyer

Institut für Physik Universität Basel, Klingelbergstrasse 82, CH-4056 Basel, Switzerland

Received 14 May 2001
Published 19 July 2001
Online at stacks.iop.org/JPhysCM/13/R619

Abstract

In this review, we present various results obtained by friction force microscopy in the last decade. Starting with material-specific contrast, commonly observed in friction force maps, we discuss how the load dependence of friction and the area of contact have been estimated and compared to elasticity theories. The features observed in a sliding process on the atomic scale can be interpreted within the Tomlinson model. An extension of the model, including thermal effects, predicts a smooth velocity dependence of friction, which recent experiments have confirmed. Other subjects like anisotropy of friction, role of environment, topographical effects, electronic friction and tip modifications are also discussed. The growing importance of molecular dynamics simulations in the study of tribological processes on the atomic scale is outlined.

Contents

0953-8984/01/310619+24$30.00

1. Introduction

Friction is a fascinating subject. In many cases, it is exploited to improve the quality of our life; for example, actions like walking, lighting a fire or playing a violin are all based on friction. On the other hand, a reduction of friction is required for machinery lubrication or skiing. In spite of its ubiquity, friction is not completely understood. A lot of facts are known from a practical point of view, but our knowledge of the intrinsic origin of friction is far from being complete. Coefficients of friction have been reported between countless couples of materials under disparate conditions, from liquid ambient to ultra-high vacuum. Nevertheless, the coefficient of friction is *not* a fundamental concept in physics.

A significant advance was realized 15 years ago, with the advent of the atomic force microscope and of its modification known as friction force microscope. With these devices, it became possible to study the sliding of a single asperity a few nanometres in size and to detect forces on the sub-nanonewton scale, which is obtained by combining the mechanical precision of piezoelectric materials and the optical sensitivity of lasers. In such a way the well known assumption that friction is proportional to the real area of contact was verified on different couples of materials, the effects of adhesive forces were quantified under various conditions and the peculiar aspects of friction on the atomic scale were extracted, understood and reproduced by theories and computer simulations.

There is not only a scientific interest in friction. The miniaturization of electronic devices is an unrestrainable process. If the linear size of a component is reduced by a factor of ten, the area of its surface diminishes ten times *less* than its volume. Thus, it is not difficult to understand why friction, which is proportional to the area of contact, is a subject of great interest also for nano-technologists. In this review, we will focus only on the experiments that, in our opinion, led to significant improvements in our knowledge of the basic mechanisms of friction. Technological applications will not be discussed in detail.

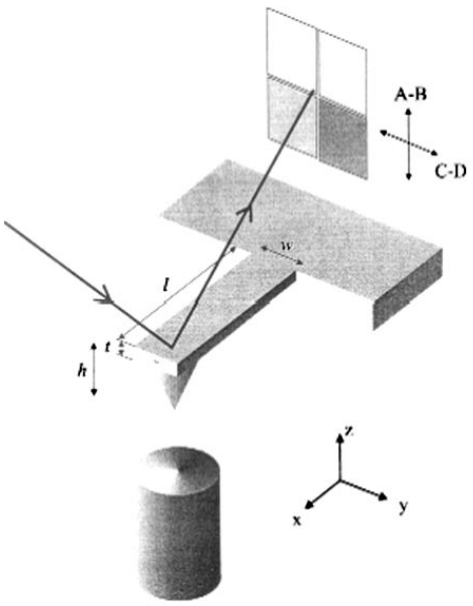

Figure 1. Schematic diagram of a beam-deflection FFM (from [3]).

2. Friction force microscopy

Since its introduction in 1986, the atomic force microscope (AFM) has turned out to be a unique tool to detect forces on length scales of atomic dimensions [1, 2]. In AFM, a sharp tip is brought into contact with a surface, which causes the normal bending of the cantilever supporting the tip (figure 1). If the tip is then shifted with respect to the sample (or vice versa), the cantilever is also twisted. Both vertical and lateral movements are realized with piezoelectric elements below the sample. The two deformations can be detected by a laser beam, which is reflected from the rear of the cantilever into a four-quadrant photodetector. The normal and lateral forces acting on the cantilever can be deduced from the normal and lateral signals acquired with the photodetector (respectively, A–B and C–D in figure 1), provided that the spring constants of the cantilever and the sensitivity of the photodetector are known [4, 5]. Alternative methods of force detection consist in capacitance detection [6], dual fibre interferometry [7] and piezoresistive sensors [8].

For rectangular cantilevers, the normal and lateral spring constants are given by $c_N = Ewt^3/4l^3$ and $c_L = Gwt^3/3h^2l$, where w, t, l are the cantilever width, thickness and length, h is the tip height and E and G are the Young's modulus and the shear modulus of the material which constitutes the cantilever [3]. The sensitivity of the photodetector is determined by measuring force–distance curves on hard surfaces, where elastic deformations can be neglected and the vertical movement of the surface is equal to the deflection of the cantilever. The calibration of cantilevers with different shape usually requires analytical evaluation or finite element analysis [9–11]. As an alternative, an *in situ* calibration of lateral forces on samples with well defined profiles is also possible [12].

When normal and lateral forces are measured at the same time, the AFM is called a friction force microscope (FFM). In such sense, the FFM tip resembles an isolated asperity of a surface, where sub-nanonewton friction forces can be easily detected. However, it is worth observing that single-asperity contacts behave in a rather different way compared with multi-asperity contacts, which are formed in the sliding of rough surfaces. The differences are discussed in section 3 in the framework of continuum mechanics.

Due to the small tip size (typical radii of curvature are below 100 nm) FFMs can be successfully used to map friction forces with extraordinary resolution. An example is given in figure 2, where some hydrocarbon islands surrounded by a fluorocarbon 'sea' are shown. The grey levels in figure 2(b) correspond to different angles of torsion and quantify the tribological response of the surface on a local scale. Incidentally, figure 2 also shows that it is possible to remove areas with the probing tip within the hydrocarbon islands, whereas the fluorocarbon sea is not destroyed by the same operation. Further examples of friction maps are presented in section 4.

The experiments discussed in sections 5 and 6 prove the applicability of continuum mechanics down to the nanometre scale. Direct measurements of friction force against applied load and indirect estimations of contact area, realized by various groups, revealed that friction forces are usually proportional to the contact area and that adhesion effects often play an important role in the sliding of the tip.

Friction on the atomic scale was measured for the first time in 1987 by Mate *et al* using a tungsten tip on graphite [2]. Two important effects were observed: (i) a saw-tooth pattern of lateral forces (*stick–slip*) and (ii) hysteresis between forward and backward scans (*friction loop*). A rather linear dependence of friction on normal force with friction coefficient $\mu = 0.01$ was also found. After this pioneering work, friction on the atomic scale was observed several times under different conditions (section 8). Figure 3 shows a typical friction loop detected on NaCl in UHV. All the features in this loop can be interpreted within the Tomlinson model [15],

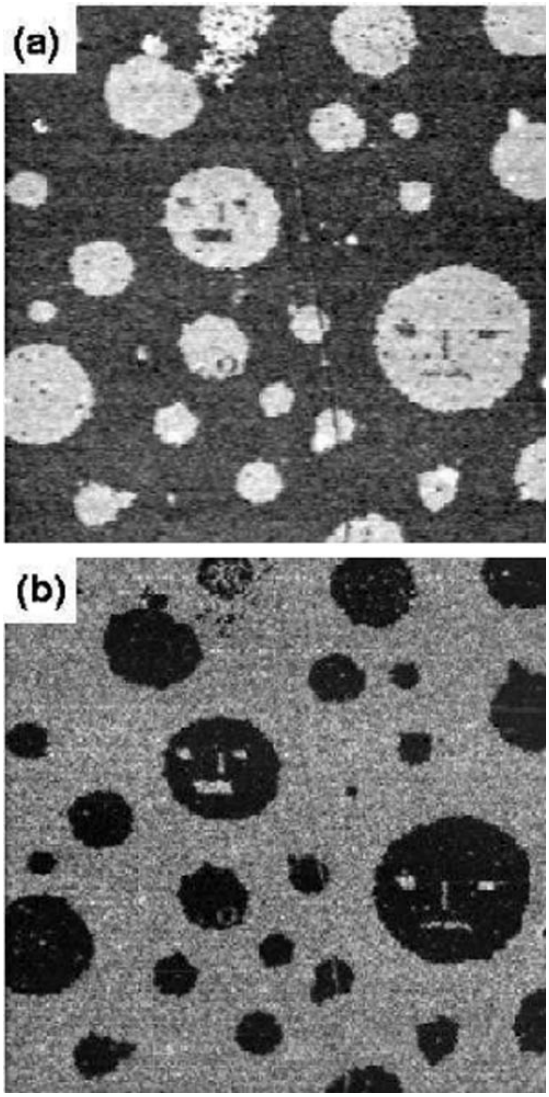

Figure 2. (a) Topography and (b) friction image of mixed Langmuir–Blodgett film (from [13]).

which is discussed in section 7. We will also show how molecular dynamics (MD) simulations of tips sliding on various surfaces can be successfully applied to interpret FFM measurements on the atomic scale. A recent extension of the Tomlinson model, which introduces temperature and velocity effects in stick–slip motion, is also presented, together with experimental results, which confirm such predictions (section 9). Other effects (anisotropy of friction, role of environment etc) are discussed in sections 10–12.

3. Single-asperity contact

On the microscopic scale, every surface is rough. If two surfaces are brought into contact, only their asperities touch each other, and the real area of contact is a few orders of magnitude

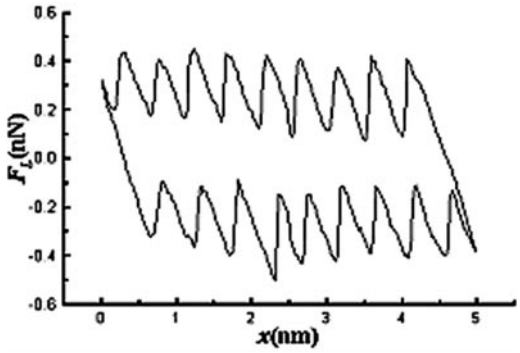

Figure 3. Friction loop detected on NaCl in UHV (from [14]).

smaller than the apparent area of contact. Furthermore, if one of the surfaces is translated with respect to the other, a dissipative friction force arises.

In 1950 Bowden and Tabor assumed that the 'lateral' friction force F_L is proportional to the real contact area, A, and to a mean lateral force per unit area, the shear strength τ: $F_L = \tau A$ [16]. If the shear strength is pressure independent, the friction force is simply proportional to the area of contact. Under zero normal loads such area is not well defined, since it depends on the length scale of the experimental apparatus. However, when a finite normal force, F_N, is applied, all structures smaller than typical length scales are destroyed due to either plastic or elastic deformation.

If the deformation is totally plastic, the asperities are compressed until the pressure becomes equal to a certain yield pressure p^* (which is usually smaller than the yield pressure of the bulk material). The resulting contact area is thus $A = F_N/p^*$, and the well known Amontons law is obtained: $F_L = \mu F_N$, where $\mu = \tau/p^*$ is the coefficient of friction. The same analysis conducted for a single asperity can be extended to contacts formed by many asperities, which leads again to the Amontons law.

Because of its simplicity, plastic deformation was assumed to explain many friction processes. However, totally plastic deformation during sliding provokes huge damage in a short time, which usually is not observed. Thus, elastic processes have an important role, too. In the case of elastic contact, the contact area between a sphere of radius R and a plane is given by

$$A(F_N) = \pi \left(\frac{R}{K}\right)^{2/3} F_N^{2/3} \tag{3.1}$$

where K is related to the Young's modulus, E, and the Poisson number, ν, of both the sphere and the plane, according to the following relation [17]:

$$\frac{1}{K} = \frac{3}{4}\left(\frac{1-\nu_1^2}{E_1} + \frac{1-\nu_2^2}{E_2}\right). \tag{3.2}$$

The result $A \propto F_N^{2/3}$ is in contrast with the Amontons law. However, a linear relationship between F_L and F_N is obtained for a multi-asperity contact if particular conditions are satisfied. Greenwood and Williamson proved that the area of contact between an exponential distribution of asperity heights (with the same radius of curvature) and a flat surface depends linearly on the normal force F_N [18]. This result is approximately valid also for a Gaussian distribution.

Adhesion has an important role, especially when measurements are not made under vacuum conditions. If the elastic deformation caused by adhesive forces is large compared

to their range of action, Johnson *et al* proved that equation (3.1) should be extended in the following way:

$$A(F_N) = \pi \left(\frac{R}{K}\right)^{2/3} (F_N + 3\pi\gamma R + \sqrt{6\pi\gamma R F_N + (3\pi\gamma R)^2})^{2/3} \tag{3.3}$$

where γ is the surface tension [19]. In the JKR model the real area of contact at zero load is finite and a negative load is required to break the contact. In contrast, if the elastic deformation is small compared to the range of adhesive forces, Derjaguin *et al* stated that

$$A(F_N) = \pi \left(\frac{R}{K}\right)^{2/3} (F_N - F_{\text{off}})^{2/3} \tag{3.4}$$

where F_{off} is a negative load required to break the contact [20]. The non-dimensional parameter

$$\Phi = \left(\frac{9R\gamma^2}{4K^2 z_0^3}\right)^{1/3} \tag{3.5}$$

where z_0 is the equilibrium distance in contact, can be used to discriminate between the JKR or DMT models. If $\Phi > 5$ the JKR model has to be applied. If $\Phi < 0.1$ the DMT model is preferable [21]. For intermediate values of Φ numerical analysis is necessary. Predictions in good agreement with experiments (section 6) are provided by the Maugis–Dugdale model [22].

Finally, it should be observed that the assumption of a pressure independent shear stress is not always fulfilled. In some cases, a linear dependence $\tau = \tau_0 + \alpha p$, where α is a dimensionless material constant, is in better agreement with experimental results [23].

4. Material-specific contrast of friction force microscopy

In their most straightforward application FFMs are used to produce tribological maps of surfaces, where friction is quantified on the nanometre scale.

In figure 4 a Langmuir–Blodgett (LB) film on a silicate substrate is mapped by contact topography and by friction force imaging [24]. The areas covered by LB film present less friction, independent of the film thickness. More complicated systems of phase separated LB films were studied by Overney *et al* [25].

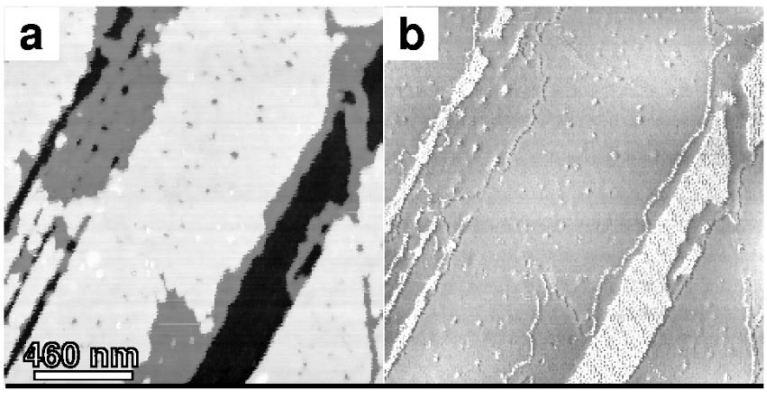

Figure 4. (a) Topography and (b) friction image of two bilayers of Cd arachidate on a silicon wafer (from [24]).

In silicon-based microdevices, low friction is required to minimize the power consumption. Scandella *et al* studied a Si(110) surface structured by standard photo-mask lithography [26]. Figure 5 shows a Si/SiO_2 grid etched in 1:100 HF/H_2O solution for a few minutes. Friction on (hydrogen passivated) silicon was found to be larger by a factor of two than friction on silicon oxide. Another example is given by Teuschler *et al*, who investigated Si(100) surfaces, patterned by the same FFM used for characterization [27]. The writing process consisted in applying a voltage to the conductive tip. An increase of friction was observed on the structured areas, where the formation of silicon oxide was reasonably enhanced. The apparent contrast with the experiment of Scandella *et al* suggests that factors like crystallinity must influence friction significantly.

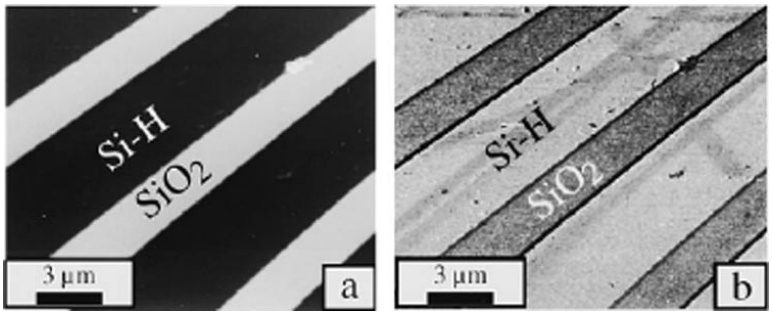

Figure 5. (a) Topography and (b) friction image of thermally grown SiO_2 stripes on Si(110) produced by optical lithography (from [26]).

Friction on III–V semiconductors was studied by Garcia and co-workers. Tamayo *et al* detected chemical variations of InP/InGaAs alloys with 3 nm resolution [28]. 10% changes in indium composition were clearly distinguished in air. The same group reported also FFM measurements with submonolayer sensitivity on quantum dot structures (InSb on InP and InAs on InP) [29].

FFM was also adopted to investigate ferroelectric materials. Lüthi *et al* [30] and Eng *et al* [31] found a significant contrast between neighbouring domains of opposite polarization in friction force maps acquired on GASH (guanidinium aluminium sulphate hexahydrate) and TGS (triglycine sulphate), respectively. On TGS Bluhm *et al* determined several different friction coefficients, depending on the polarization, the asymmetry of the surface potentials and also the orientation of the crystallographic lattice with respect to the scan direction [32]. On GASH, the contrast was related only to structural differences, which modify the surface potential experienced by the FFM tip. Furthermore, it was proven that electrostatic interactions between tip and sample did not affect significantly the friction force.

Lüthi *et al* [33] and Schwarz *et al* [23] performed nanotribological studies on C_{60} islands. The former analysis revealed that friction in UHV is much higher on C_{60} islands than on the underlying NaCl substrate; the latter showed a load dependence of Hertzian type, which was probably due to capillary condensation (the experiment was performed in air). However, the main result is that C_{60} islands could be moved with respect to the substrate with extraordinary low shear strength $\tau = 0.05$–0.1 MPa [34]. Thus, Lüthi *et al* suggested a possible application of C_{60} islands as a sled-type transport system on the nanometre scale (figure 6).

Recently, Bluhm *et al* observed friction on a nanometre thin ice film grown on mica. A friction coefficient $\mu = 0.60$ was measured in the temperature range from -24 to $-40\,^{\circ}C$ [35]. This value is comparable to the static friction measured in macroscopic experiments [16]. Thus, dry friction was probably revealed, due to the squeezing of the water layer out

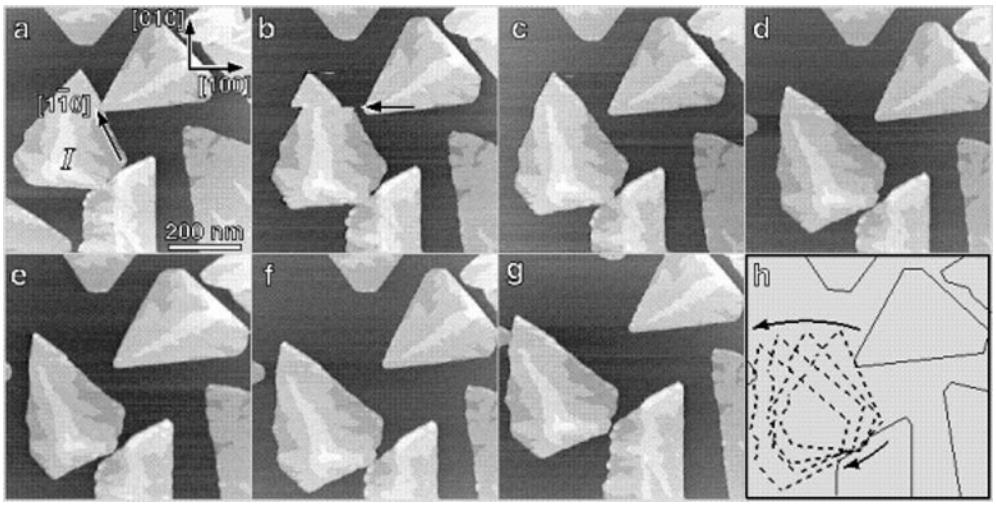

Figure 6. A sequence of 530 nm by 530 nm top-view AFM images are shown. The dark area corresponds to the NaCl(001) substrate, whereas the bright areas are C_{60} islands (from [34]).

of the contact, observed when the AFM is operated in non-contact mode. Other effects like pressure melting and frictional heating were found to be not significant.

5. Load dependence of friction

The discussion presented in section 3 suggests that a non-linear dependence on the applied load is expected in FFM experiments, except in the case of multi-asperity contacts. With well defined spherical tips, Schwarz *et al* obtained the DMT relation (3.4) on graphite, diamond, amorphous carbon and C_{60} in argon atmosphere (figure 7). As the friction coefficient μ is not applicable for comparing the tribological behaviour of different materials in such a case, the authors suggested the introduction of an 'effective friction coefficient for point-contact-like single-asperity friction', independent of the tip curvature. Enachescu *et al* found the DMT relation in UHV, using a tungsten carbide tip on diamond [37, 38]. Their result is reasonable due to the extreme hardness of the sample.

UHV measurements in agreement with JKR theory were performed by Meyer *et al* on NaCl [39], Carpick *et al* on mica [40] and Polaczyk *et al* on Au(100) [41]. To extract the load dependence of friction Meyer *et al* applied an original 2D histogram technique, which allows investigation of the correlation between lateral and normal forces with improved statistics. Carpick *et al* pointed out that for non-spherical tips the JKR relation (3.3) has to be modified. In the case of an axisymmetric tip profile $z \propto r^{2n}$ $(n > 1)$ a slow increase of the contact area can be found analytically.

Altogether, these results lead to an important conclusion: continuum mechanics can be applied for tip radii down to a few nanometres.

6. Estimation of the contact area

In contrast to other tribological instruments, like the surface force apparatus [42, 43], the contact area cannot be directly measured by FFM. However, a satisfying indirect method

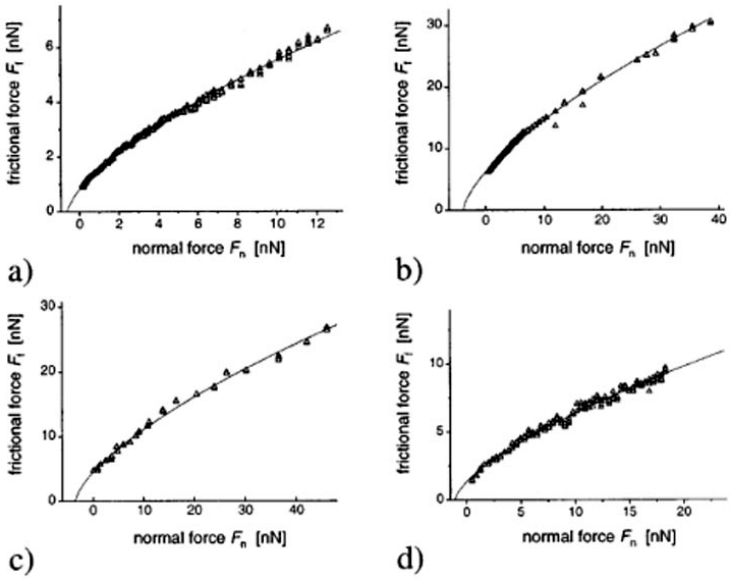

Figure 7. Friction–load curve on amorphous carbon in argon atmosphere. Panels (a)–(d) refer to tips with different radii of curvature (from [36]).

relies on lateral stiffness measurements. According to various models, the lateral stiffness of the contact between a sphere and a plane is given by [44]

$$k^x_{\text{contact}} = 8aG^* \tag{6.1}$$

where a is the contact radius and

$$\frac{1}{G^*} = \frac{2-\nu_1^2}{G_1} + \frac{2-\nu_2^2}{G_2} \tag{6.2}$$

(G_1, G_2 and ν_1, ν_2 are the shear modulus and the Poisson number of the two materials). The contact between the FFM tip and the sample can be modelled by a series of three lateral springs (figure 8). The effective constant k^x_{eff} of the series is given by

$$\frac{1}{k^x_{\text{eff}}} = \frac{1}{k^x_{\text{contact}}} + \frac{1}{k^x_{\text{tip}}} + \frac{1}{c_L} \tag{6.3}$$

where k^x_{contact} and k^x_{tip} are the lateral stiffness of the contact and of the tip, and c_L is the lateral spring constant of the cantilever. The effective spring constant k^x_{eff} is deduced from the slope of the 'sticking' part of the friction loop, as we will show in section 7.1. Thus, the contact radius a can be easily estimated by equation (6.1).

Carpick *et al* measured the lateral stiffness of the contact between silicon nitride tip and muscovite mica in air [45]; Lantz *et al* applied this method to $NbSe_2$ and graphite in UHV [46, 47]. In both cases friction measurements were also performed. As a result, it was found that the same fitting models could be applied to both the spring constant k^x_{eff} and the lateral force F_L. The JKR model [19] is in agreement with the experiment of Carpick *et al*, and the Maugis–Dugdale model [22] with the experiment of Lantz *et al*. Thus, the friction force and the contact area are proportional in the applied range of loads (up to $F_N = 40$ nN in both experiments).

An independent way to estimate the contact area was explored by Enachescu *et al*, who measured the contact conductance as a function of the applied load on diamond [37, 38]. Their

Figure 8. Lateral stiffness in FFM. The contribution of the tip is neglected (from [45]).

results can be fitted with a DMT relation, similarly to friction–load dependence. As the contact conductance is proportional to the contact area, the proportionality between friction and contact area was confirmed again.

It is worth observing that proportionality between friction and contact area is also predicted in MD simulations at ultra-low loads. In a systematic study on copper surfaces, Sørensen *et al* found a linear increase of friction with the number of atoms in the bottom layer of a flat Cu(111) tip sliding on a Cu(111) surface; however, the two surfaces have to be oriented in the same way [48].

7. Friction on the atomic scale

7.1. The Tomlinson model at zero temperature

In 1929 Tomlinson suggested that the dissipation in friction is due to a stick–slip mechanism [15]. Like a violinist, who creates sounds moving a sticky bow on a string, the FFM produces friction with a silicon tip. Stick–slip on the atomic scale has been studied theoretically by various groups [49–53]. Here, we derive the main results of the Tomlinson model in one dimension, without the influence of thermal effects. An extension of the Tomlinson model in two dimensions is discussed in [50, 54].

The FFM tip is subject to a potential $V_{\rm tot}(x,t)$ equal to the sum of the periodic potential describing the tip–sample interaction and the elastic potential of the cantilever. Assuming a sinusoidal shape for the first term of the sum, we can write

$$V_{\rm tot}(x,t) = -\frac{E_0}{2}\cos\frac{2\pi x}{a} + \frac{1}{2}k^x_{\rm eff}(x-vt)^2 \tag{7.1}$$

where E_0 is the peak-to-peak amplitude of the tip–sample potential, a is the lattice constant of the surface, $k^x_{\rm eff}$ is the effective lateral spring constant and v is the velocity of the support. In figure 9, the total potential $V_{\rm tot}(x,t)$ is shown at different instants t. The adopted values are typical of FFM experiments.

The tip is localized in the first position $x = x_{\rm min}$ where the first derivative of $V_{\rm tot}(x,t)$ with respect to x is zero:

$$\frac{\partial V_{\rm tot}}{\partial x} = \frac{\pi E_0}{a}\sin\frac{2\pi x}{a} + k^x_{\rm eff}(x-vt) = 0. \tag{7.2}$$

Using the approximation $\sin\alpha \approx \alpha$ in equation (7.2), we obtain the initial velocity of the tip,

$$v_{\rm tip}(0) = \left.\frac{{\rm d}x_{\rm min}}{{\rm d}t}\right|_{t\to 0} = \frac{v}{1+\gamma} \tag{7.3}$$

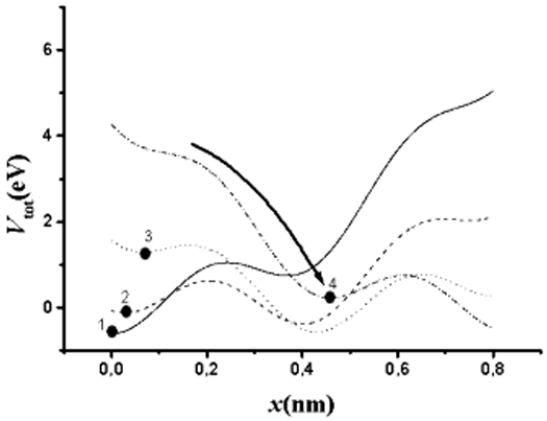

Figure 9. Potential describing the FFM tip sliding over a periodic surface at different instants ($E_0 = 1.22$ eV, $k_{\text{eff}} = 2.78$ N m^{-1}, $a = 0.42$ nm, $v = 50$ nm s^{-1}).

where

$$\gamma = \frac{2\pi^2 E_0}{k_{\text{eff}}^x a^2}. \tag{7.4}$$

With the values adopted in figure 9, $\gamma = 7.86$ and $v_{\text{tip}}(0) = 5.65$ nm s^{-1}, which is much less than the cantilever velocity, $v = 50$ nm s^{-1}.

The jump of the tip occurs at the position $x_{\min} = x^*$, where the second derivative of the total potential with respect to x is zero:

$$\frac{\partial^2 V_{\text{tot}}}{\partial x^2} = \frac{2\pi^2 E_0}{a^2} \cos \frac{2\pi x}{a} + k_{\text{eff}}^x = 0 \tag{7.5}$$

which gives

$$x^* = \frac{a}{2\pi} \arccos\left(-\frac{1}{\gamma}\right). \tag{7.6}$$

The lateral force $F^* = -k_{\text{eff}}^x(x^* - vt)$, which induces the jump, can be evaluated by equations (7.2) and (7.5), using the identity $\cos^2\alpha + \sin^2\alpha = 1$:

$$|F^*| = \frac{k_{\text{eff}}^x a}{2\pi}\sqrt{\gamma^2 - 1}. \tag{7.7}$$

Thus, the stick–slip is observed only if $\gamma > 1$ (soft cantilever or strong tip–sample interaction). With the values in figure 9, $x^* = 0.114$ nm and $|F^*| = 1.45$ nN. The lateral force can be evaluated also when $t \to 0$:

$$|F_L(0)| = \frac{\gamma}{\gamma + 1} k_{\text{eff}}^x vt. \tag{7.8}$$

If $\gamma \gg 1$, the effective lateral spring constant is approximately given by the ratio $|F_L(0)|/vt$.

Another important quantity is the energy barrier $\Delta E^+(t)$, defined as $\Delta E^+(t) = V(x_{\max}(t), t) - V(x_{\min}(t), t)$. In figure 10 the energy barrier ΔE^+ is plotted as a function of the lateral force $|F_L|$. In a small range not too close to the critical point, we can assume that

$$\Delta E^+(t) = \lambda |F^* - F_L| \tag{7.9}$$

where λ is a constant parameter [55].

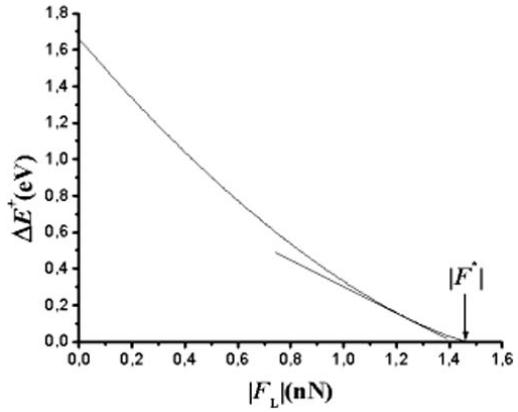

Figure 10. Lateral force dependence of the energy barrier ΔE^+.

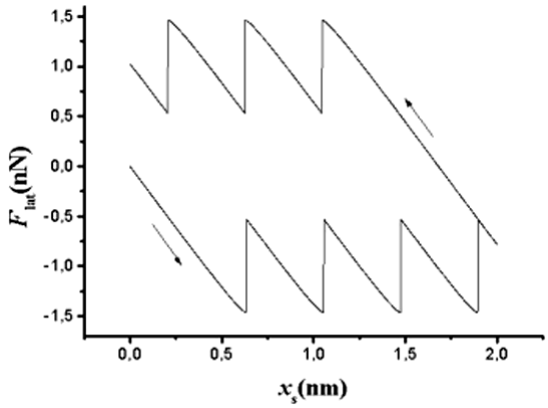

Figure 11. Theoretical friction loop at $T = 0$.

The initial slope of the curve $\Delta E^+ = \Delta E^+(t)$ is

$$\left.\frac{\mathrm{d}}{\mathrm{d}t}\Delta E^+(t)\right|_{t\to 0} = -k^x_{\mathrm{eff}} v x_{\max}(0) \approx -k^x_{\mathrm{eff}} \frac{a}{2}\frac{\gamma}{\gamma-1} v \tag{7.10}$$

so that

$$\lambda \lesssim \frac{a}{2}\frac{\gamma+1}{\gamma-1}. \tag{7.11}$$

At $t^* = 12.7$ ms the tip 'jumps' and reaches the next local minimum of the total potential, $x_{\min} = x'^*$. At this point, the lateral force is $F'^*_L = -k_{\mathrm{eff}}(x'^* - vt^*)$. The corresponding lateral force F'^*_L can be estimated assuming that $x'^* = a + \delta x$ and using $\sin\alpha \approx \alpha$, which leads to $\delta x \approx (vt^* - a)/(\gamma + 1)$ and $F'^*_L \approx \gamma k^x_{\mathrm{eff}} \delta x$. With the values in figure 9, $F'^* = 0.531$ nN. A jump $\Delta F_L = F'^*_L - F^*_L = 0.92$ nN has occurred.

After the first jump the lateral force F_L increases again and new jumps of the tip are induced when $F_L = F^*_L$. If the direction of the support is suddenly reversed the lateral force F_L decreases and, when $F_L = 0$, the situation is exactly the same we had at $t = 0$, except for the opposite direction. Figure 11 shows the result of a forward and backward scan, i.e. the lateral force F_L as a function of the support position, x_s.

7.2. The Tomlinson model at finite temperature

At finite temperature T, the lateral force, F_L, which is necessary to induce a jump, is less than the value determined at zero temperature (equation (7.7)). Such a force is not fixed, but statistically distributed around a mean value $F_L^*(T)$. To estimate $F_L^*(T)$, we have first to evaluate the probability $p(t)$ that the tip does not jump, which can be found using the master equation

$$\frac{\mathrm{d}p(t)}{\mathrm{d}t} = -f_0 \exp\left(-\frac{\Delta E^+(t)}{k_B T}\right) p(t). \tag{7.12}$$

In equation (7.12), ΔE^+ is the energy barrier, previously discussed, and f_0 is the characteristic transversal frequency of the system. Note that the probability of a reverse jump is neglected in equation (7.12), as in such a case the energy barrier to overcome is much higher than ΔE^+.

To evaluate the lateral force corresponding to the maximum jump probability, we make a change of variable replacing time by the corresponding lateral force. The master equation becomes

$$\frac{\mathrm{d}p(F_L)}{\mathrm{d}F_L} = -f_0 \exp\left(-\frac{\Delta E^+(F_L)}{k_B T}\right)\left(\frac{\mathrm{d}F_L}{\mathrm{d}t}\right)^{-1} p(F_L). \tag{7.13}$$

At this point, we substitute

$$\frac{\mathrm{d}F_L}{\mathrm{d}t} = \frac{\mathrm{d}F_L}{\mathrm{d}x_s}\frac{\mathrm{d}x_s}{\mathrm{d}t} \approx k_{\mathrm{eff}}^x v \tag{7.14}$$

and use the approximation (7.9). The maximum probability transition condition,

$$\frac{\mathrm{d}^2 p(F_L)}{\mathrm{d}F_L^2} = 0 \tag{7.15}$$

then yields (at fixed temperature)

$$F_L^*(v) = \frac{k_B T}{\lambda} \ln \frac{v}{v_1} + \mathrm{const} \tag{7.16}$$

with $v_1 = 1$ nm s^{-1}. Thus, the lateral force depends logarithmically on the sliding velocity. It is important to observe that the approximation (7.9) is valid if the tip jumps not too close to the critical point $x = x^*$, which is not the case at high velocities. In such a case equation (7.14) implies that the factor $(\mathrm{d}F_L/\mathrm{d}t)^{-1}$ is small and, consequently, the probability $p(t)$ does not change significantly. Thus, friction is constant at high velocities. The critical velocity v_c, which discriminates between the two regimes, depends on the characteristic frequency f_0. It is not difficult to prove that

$$v_c \approx \frac{f_0 k_B T}{k_{\mathrm{eff}}^x \lambda}. \tag{7.17}$$

Assuming $f_0 = 212$ kHz (the fundamental torsional frequency of a standard cantilever, see [56]) we conclude that $v_c > \sim 1.4\ \mu$m s^{-1}.

7.3. Molecular dynamics simulations

Several authors have studied sliding friction on the atomic scale using molecular dynamics (MD). Their results are useful to interpret experimental data, and also to suggest new experiments.

Landman *et al* found atomic-scale stick–slip for a Si tip sliding on a Si(111) surface [57] and for a CaF_2 tip on a CaF_2 substrate [58]. Harrison *et al* predicted the same effect for

two hydrogen-terminated diamond (111) surfaces and also a weak dependence on load [59], in a certain agreement the experiments realized by Germann *et al* (section 8). In their MD simulations, Sørensen *et al* observed the occurrence of wear on Cu(100) surfaces, whereas Cu(111) seemed to be more resistant to the sliding of an asperity [48]. This effect was also found experimentally by Bennewitz *et al* (section 8).

Shluger *et al* proved that the scanning process is accompanied by strong displacements of the surface ions inside the lattice, and by their transient or permanent adsorption onto the tip at low loads (up to 1 nN) [60–62]. However, a recent simulation by Livshitz and Shluger suggested that the adsorbed material could adjust itself (figure 12) leading to a self-lubrication effect [63], which is consistent with the periodic structures observed in the experiments also at rather high loads (section 8).

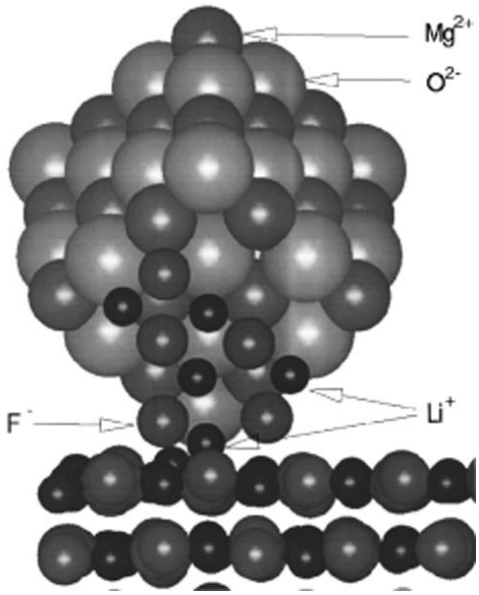

Figure 12. Regular structure of ions adsorbed on a MgO tip sliding on a LiF surface (from [63]).

Ohzono and Fujihira have recently simulated friction between an ordered organic monolayer composed of *n*-alkane molecules and a rigid slider with a single protuberance [64, 65]. As a result, they found that incommensurability at the interface and tip size comparable to the molecular size should be important conditions in imaging the molecular lattice, in agreement with experiments of Takano *et al* (section 10).

Finally, recent MD simulations studied in detail the connection between friction and wear on the nanometre scale. Buldum *et al* simulated the effects of the indentation and the sliding of sharp and blunt Ni tips on Cu(111) and Cu(100) surfaces [66]. The sliding of the sharp tip induces two consecutive structural transformations that occur periodically, but end with the wear of a layer. For the blunt tip the stick–slip is less regular.

Komanduri *et al* considered the Al(100) surface scratched at very small depths (to 0.8 nm) [67]. A rather high friction coefficient $\mu = 0.6$ was found, independent of the scratch depth, which is probably related to the finite value of the scratch force involved in breaking and reforming of the atomic bonds.

8. Friction experiments on the atomic scale

Friction on ionic crystals was systematically studied by E Meyer and coworkers with an UHV–FFM apparatus [14, 68–71], which made possible the detection of atomic stick slip on NaF, NaCl, AgBr and KBr with standard silicon tips.

In figure 13 a friction map obtained on KBr(100) is compared with a theoretical map, determined with the 2D Tomlinson model. The slope of the sticking part in figure 13(c) is about $k^x_{\rm eff} = 7$ N m^{-1}. According to the analysis presented in section 6, this value, combined with the lateral spring constant, $c_L = 35.5$ N m^{-1}, and the lateral stiffness of the tip, $k^x_{\rm tip} = 84$ N m^{-1}, leads to $k^x_{\rm contact} = 18$ N m^{-1}. Using $G_{\rm KBr} = 1.0 \times 10^{10}$ N m^{-2}, $\nu_{\rm KBr} = 0.25$, $G_{\rm Si} = 6.8 \times 10^{10}$ N m^{-2} and $\nu_{\rm Si} = 0.22$, a contact radius $a = 0.42$ nm is estimated, at the limit of continuum theory.

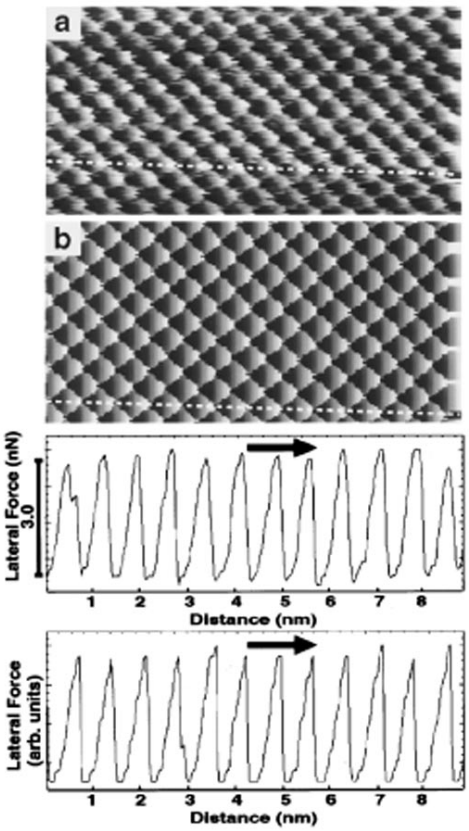

Figure 13. (a) Experimental and (b) theoretical friction image of KBr(100) (from [71]).

Special tips covered by PTFE (polytetrafluoroethylene) made possible the observation of atomic features on the reconstructed Si(111)7 × 7 surface [72]. Due to the lubricant properties of PTFE, adhesion and friction are significantly reduced; furthermore, PTFE does not react with the dangling bonds of Si(111)7 × 7. In contrast, uncoated Si tips, and tips coated with Pt, Au, Ag, Cr and Pt/C damaged the sample irreversibly.

With the same UHV–FFM Bennewitz *et al* measured atomic stick–slip on copper [73, 74]. A reproducible stick–slip was detected on the Cu(111) surface, whereas irregularity and scarce

reproducibility of results were found on the Cu(100) surface (figure 14). MD simulations by Sørensen *et al* proved that sliding without wear occurs preferably on the close packed Cu(111) surface rather than on Cu(100) [48]. In these simulations, Cu tips were used. Thus, in the experiments of Bennewitz *et al* the FFM tip was reasonably covered by copper. This hypothesis is supported by the weak load dependence of friction and by current measurements, as explained in [73].

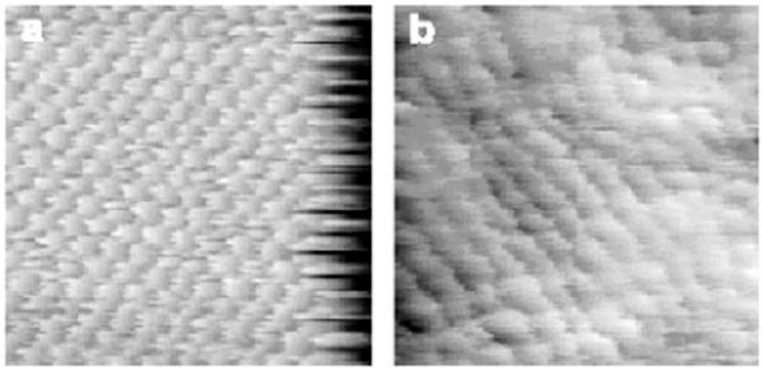

Figure 14. Friction images of (a) Cu(111) and (b) Cu(100). Scan size: 3 nm (from [74]).

Atomic stick–slip on the hard diamond (100) and (111) surfaces was first observed by Germann *et al* with an apposite diamond tip in UHV [75]. Subsequently, van der Oetelaar and Flipse measured friction on hydrogen-terminated (1×1) diamond (111) with silicon tips [76]. The removal of hydrogen from the surface gave rise to an enormous increase of friction.

Fujisawa *et al* measured friction on mica, MoS_2 and NaF with a 2D FFM apparatus, which revealed friction forces also perpendicularly to the scan direction [77, 78]. This effect is a consequence of the zig-zag walk of the tip, which can be predicted within the 2D Tomlinson model [50]. It is remarkable that the 2D stick–slip on NaF was limited to loads below 14 nN, whereas loads up to 10 μN could be applied on layered materials. Thus, the 2D stick–slip on NaF is related to a few-atom contact. The zig-zag walk on mica was confirmed by Kawakatsu and Saito using an original 2D FFM with two laser beams and two quadrant photodetectors [79].

9. Velocity dependence of friction

The velocity dependence of friction on the atomic scale was recently studied by Gnecco *et al* on NaCl [14]. It was proven that the atomic stick–slip varies according to a logarithmic law at low velocities ($v < 1$ μm s^{-1}) (figure 15), as predicted by the thermally activated Tomlinson model discussed in section 6.2. A comparison with equation (7.16) leads to $\lambda = 0.25$ nm for $F_N = 0.44$ nN and $\lambda = 0.14$ nm for $F_N = 0.65$ nN, consistently with equation (7.11). A logarithmic dependence on velocity was also reported by Bennewitz *et al* on Cu(111) [73].

The velocity dependence of friction on the micrometre scale was studied by Bouhacina *et al* [80] and by Zwörner *et al* [81]. In the first experiment both triethoxysilane molecules and polymers grafted on silica showed a linear increase of the friction force with the logarithm of the sliding velocity up to $v = 300$ μm s^{-1}. This result was interpreted within a thermally activated Eyring model [82, 83]. Zwörner *et al* reported that friction between silicon tips and different carbon compounds (diamond, graphite and amorphous carbon) is constant in the

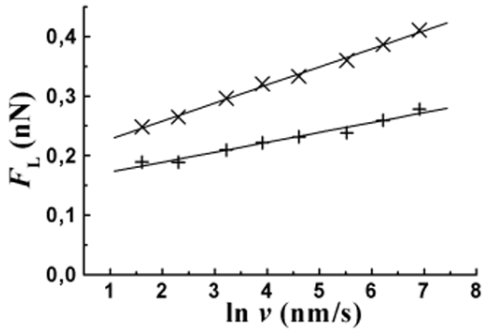

Figure 15. Mean friction force against scanning velocity on NaCl(100) at $F_N = 0.44$ nN (+) and $F_N = 0.65$ nN (×).

μm s^{-1} range. However, their experimental data also reveal a small decrease of friction when v tends to zero. We have proven that the mechanism of thermal activation is not relevant when the sliding velocity exceeds a critical value v_c, so that friction becomes independent of velocity. The critical velocity depends on several parameters, i.e. amplitude of the tip–sample potential, applied load, temperature and a characteristic frequency f_0 (equation (7.17)). Thus, it cannot be excluded that v_c lay in the velocity range explored by Zwörner *et al*. An experiment in which both regimes are observed was reported by Gourdon *et al*, who measured the velocity dependence of friction on LB films within the velocity range 0.01 to ∼50 μm s^{-1} [84]. The critical velocity $v_c = 3.5$ μm s^{-1} was interpreted as the transition between a static and sliding friction regime.

10. Anisotropy of friction

The role of the sliding direction in friction processes was clearly observed by Hirano *et al* in the contact of two mica sheets with different orientations [85]. Overney *et al* realized the first measurements of friction anisotropy by FFM on an organic bilayer film and proved that different molecular alignments lead to a significant change of friction [86]. Further measurements of friction anisotropy on stearic acid single crystals have been reported by Takano and Fujihira [87].

An impressive example of friction anisotropy is given by thiolipid LB films [84, 88]. Gourdon *et al* observed a flower-shaped island, formed by domains with different molecular orientation (figure 16). The dependence of friction on direction suggested that molecules have radial tilt, which is directed towards the centre of the 'flower'.

In the context of nanosled experiments, Sheehan and Lieber observed that MoO_3 islands on NoS_2 slide only along low index MoS_2 directions [89]. In contrast, Lüthi *et al* found that friction is independent of direction for the case of C_{60} islands on NaCl [34]. Such different behaviour is probably due to the large mismatch of C_{60} on NaCl, which should give a weak dependence of orientation ([3], p 312).

A recent example of friction anisotropy is related to carbon nanotubes (CNTs). Falvo *et al* manipulated CNTs on graphite using an AFM tip [90, 91]. A dramatic increase of lateral force was found in certain discrete directions, corresponding to transitions from incommensurate to commensurate states. At the same time the CNT motion changed from sliding/rotating to stick–roll.

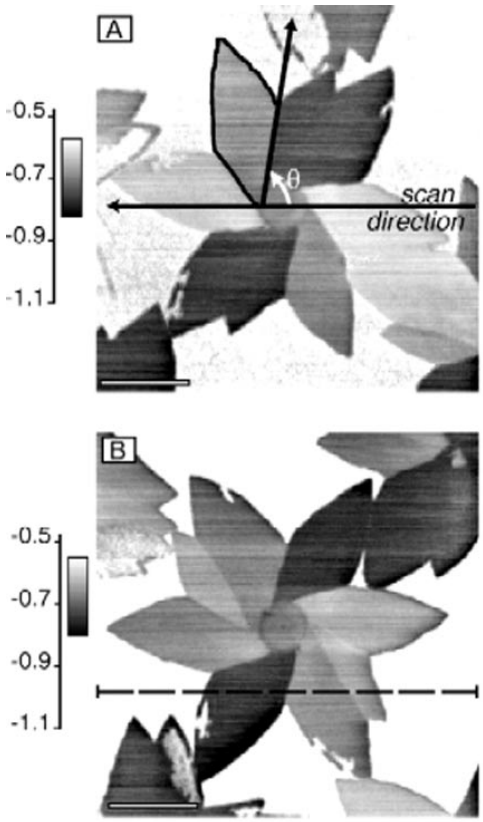

Figure 16. Friction images of a thiolipid monolayer on a mica surface. (Reprinted with permission from [88]. Copyright 1998 American Association for the Advancement of Science).

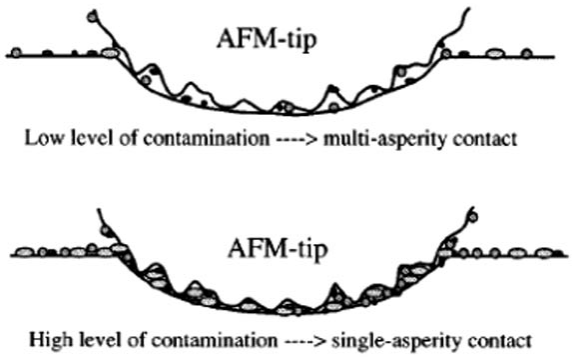

Figure 17. Influence of humidity on FFM measurements (from [95]).

11. Role of environment

The role of environment in nanotribology is fundamental. A humidity increase can provoke the formation of water layers on hydrophilic surfaces, which cause capillary interaction with the tip [92]. Thus, the conditions under which FFM measurements are realized should be always specified.

The influence of capillary condensation and humidity in FFM measurements was first studied by Binggeli and Mate using a tungsten tip [93]. A substantial decrease in adhesion and friction, observed on a hydrophilic silicon oxide surface at humidities above 70%, was related to strong capillary formation. On less hydrophilic amorphous carbon films and lubricated silicon oxide, the decrease was observed only in adhesive forces. A reduction of friction on mica at humidities above 70% was also reported by Hu *et al* [94].

Putman *et al* studied the sliding of a Si_3N_4 tip on mica and glass in different environments, from ambient to N_2 or Ar gas conditions [95]. In ambient conditions, the friction–load curves showed the Hertzian behaviour $F_L \propto F_N^{2/3}$. For the same tip under gaseous conditions the friction force increased linearly with the load, indicating multi-asperity contact. A reasonable explanation of this result is that the tip was smoothed by a condensed water film, which led to a single asperity contact at high humidities and to a multi-asperity contact at low humidities (figure 17).

Schumacher *et al* performed a systematic study of the humidity dependence of friction between standard FFM tips and single-layer MoS_2 deposited on mica or AlO_3 [96]. At 40% humidity an ordered layer of adsorbed water was formed, which led to a strong increase in friction on the strongly hydrophilic mica (figure 18). The Hertzian dependence $F_L \propto F_N^{2/3}$ was also observed. However, friction decreased above 60%, probably because water acted as a boundary lubricant. Friction on other surfaces (MoS_2 and AlO_3) revealed only slight humidity dependence. An increase of friction at ∼40% humidity was also reported by Xu *et al* on NaCl [97].

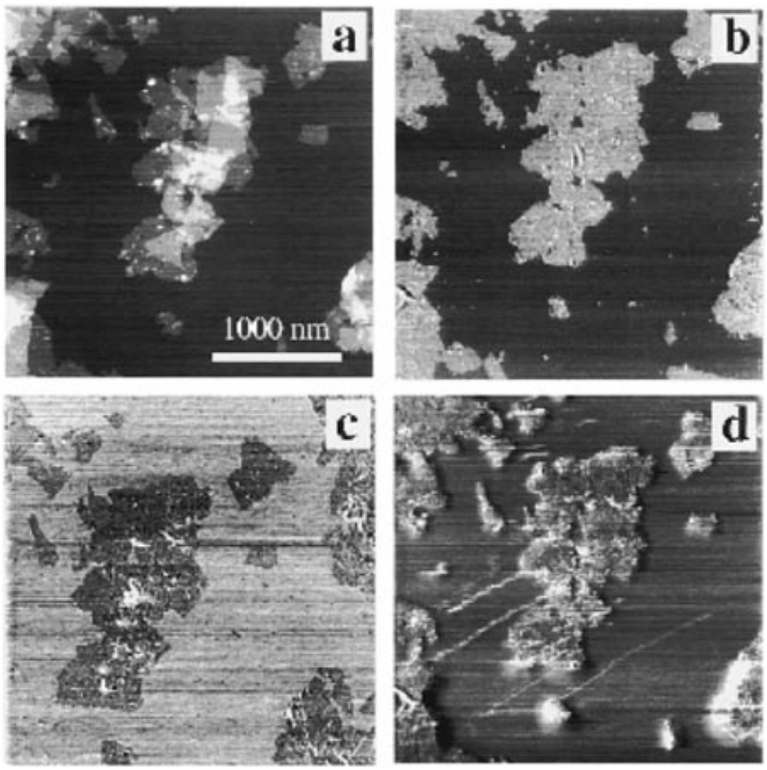

Figure 18. (a) Topography image of MoS_2 single layers deposited on a mica substrate. Friction image at (b) 10%, (c) 40% and (d) 80% humidity. Note the contrast reversal at 40% (from [96]).

Marti *et al* found a strong influence of the pH in the sliding of a silicon nitride tip on an oxidized silicon surface under aqueous electrolyte solutions [98]. As a possible application, it was suggested that many chemical species on surfaces could be differentiated using FFM by varying the pH value of the surrounding medium.

12. Other effects

12.1. Role of topography

We have considered the sliding of the tip only on flat surfaces. For rough surfaces the lateral force acquired by FFM is not equal to the friction force. In such cases the local slope of the topography and local variations of the contact area often give a significant contribution to the lateral force maps acquired by FFM. The non-dissipative part of the lateral forces due to the former topography effect can be easily separated by subtracting back and forward scans. The latter effect is due to changes of long-range forces and contact area and it is more difficult to separate.

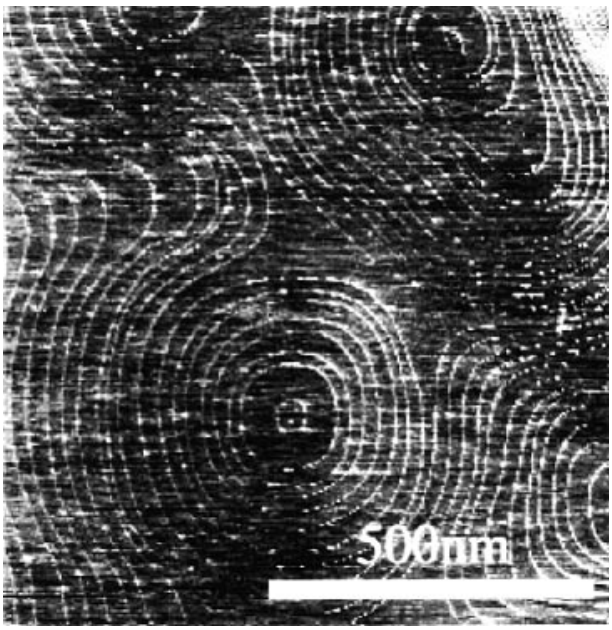

Figure 19. Friction image of NaCl. Increased friction is observed on the step sites, both going down and up the step, which indicates that the friction at the step edge is not dominated by topography effects (from [39]).

Friction at step edges is a particular topographic effect. It is influenced by several factors as variations of contact area and differences in van der Waals, capillary and electrostatic forces. Focusing on the atomistic mechanisms, both G Meyer and Amer [5] and E Meyer *et al* [39] found that friction detected on NaCl under UHV conditions is larger on step edges than on terraces (figure 19). This effect can be explained in terms of increased energy barriers at the steps, known as Schwoebel barriers.

12.2. Electronic friction

The importance of an electronic contribution to friction processes was theoretically outlined by Persson, who considered the adsorption of small particles of mass m on a thin conducting film [99]. In such a case an electronic friction force $F_{L,\mathrm{el}} = m\eta_{\mathrm{el}}v$ gives rise to an additional resistivity

$$\Delta\rho = \eta_{\mathrm{el}}\frac{mn_a}{(ne)^2 d} \tag{12.1}$$

where n is the number of conduction electrons per unit volume, n_a is the coverage of the adsorbed particles and d is the film thickness. Experiments in agreement with this effect were performed by Krim *et al*, who related the tribological properties of thin adsorbed films to changes of the Q-factor of a quartz crystal microbalance [100]. In such way, it was found that slip times for chemisorbed oxygen/silver surfaces are longer than those for silver, arguing that electronic contributions to friction should be considered whenever conducting surfaces are involved [101].

More recently, Dayo *et al* proved that friction of incommensurate N_2 on lead drops abruptly at the superconducting transition temperature $T_c \approx 5$ K, which was related again to an electronic contribution to friction [102]. However, Persson *et al* pointed out that in the experiment a lead/lead oxide/hydrocarbon composite system was reasonably formed, which leads to difficulties in the theoretical interpretation of the results [103].

The existence of an electronic contribution to the mechanism of energy dissipation at the sliding interface of a solid–solid point contact was pointed out by Merrill and Perry, who studied the effect of oxygen adsorption on vanadium carbide(100) in UHV [104]. The coefficient of friction with respect to a standard FFM tip was reduced by 40%, which was associated with the reduction in the density of metal d electrons nearest the Fermi level after oxygen adsorption.

12.3. Tip modifications

Frisbie *et al* used molecularly modified FFM tips and organic monolayers to detect friction between CH3/CH3, CH3/COOH, and COOH/COOH functional groups [105]. Depending on the functional group, different contrasts were observed. Other FFM measurements performed with chemically modified tips are reported in [106, 107].

Besides chemical modifications, other changes can affect the geometry of the tip. Instead of using sharp tips, Ando *et al* studied friction and adhesion with flat tips 0.7 μm in size [108, 109]. In such way, it was found that the pull-off force was proportional to the radius of curvature of sub-micrometre silicon asperities, in agreement with JKR and DMT models.

A singular experiment was recently realized by Heim *et al*, who measured rolling friction forces in a chain of silica microspheres fixed between the end of a tipless cantilever and a microscopy slide [110]. Rolling friction was found to be two orders of magnitude lower than adhesion, proportional to the sphere radii.

13. Conclusion

We have emphasized the variety of friction processes, involved in different physical systems, which have been investigated and understood by friction force microscopy. The unique opportunity to detect and control forces acting between a sharp nanometre-sized tip and a surface has been exploited to study the interaction of interfaces down to the atomic scale, and a lot of information has been extracted, also at a fundamental level (load and velocity dependence of friction).

Although the reported experiments constitute a significant breakthrough in our comprehension of tribology, much work is still to be done. Subjects like temperature dependence of friction, or friction changes in phase transitions require further investigation. The subject of friction is extremely wide, and we believe that the observation of nature and the needs of technology will suggest new exciting experiments in this field.

References

[1] Binnig G, Quate C F and Gerber Ch 1986 *Phys. Rev. Lett.* **56** 930
[2] Mate C M, McClelland G M, Erlandsson R and Chiang S 1987 *Phys. Rev. Lett.* **59** 1942
[3] Meyer E, Overney R M, Dransfeld K and Gyalog T 1998 *Nanoscience: Friction and Rheology on the Nanometer Scale* (Singapore: World Scientific)
[4] Marti O, Colchero J and Mlynek J 1990 *Nanotechnology* **1** 141
[5] Meyer G and Amer N 1990 *Appl. Phys. Lett.* **57** 2089
[6] Neubauer G, Cohen S R, McClelland G M, Horn D E and Mate C M 1990 *Rev. Sci. Instrum.* **61** 2296
[7] Rugar D, Mamin H J and Güthner P 1989 *Appl. Phys. Lett.* **55** 2588
[8] Linnemann R, Gotszalk T, Rangelow I W, Dumania P and Oesterschulze E 1996 *J. Vac. Sci. Technol.* B **14** 856
[9] Neumeister J M and Ducker W A 1994 *Rev. Sci. Instrum.* **65** 2527
[10] Warmack R J, Zhen X-Z, Thundat T and Allison D P 1994 *Rev. Sci. Instrum.* **65** 394
[11] Sader J E 1993 *Rev. Sci. Instrum.* **66** 4583
[12] Ogletree D F, Carpick R W and Salmeron M 1996 *Rev. Sci. Instrum.* **67** 3298
[13] Meyer E *et al* 1992 *Thin Solid Films* **220** 132
[14] Gnecco E, Bennewitz R, Gyalog T, Loppacher Ch, Bammerlin M, Meyer E and Güntherodt H-J 2000 *Phys. Rev. Lett.* **84** 1172
[15] Tomlinson G A 1929 *Phil. Mag.* **7** 905
[16] Bowden F P and Tabor D 1950 *The Friction and Lubrication of Solids* (Oxford: Oxford University Press)
[17] Landau L D and Lifshitz E M 1998 *Introduction into Theoretical Physics* vol 7 (Moscow: Nauka)
[18] Greenwood J A and Williamson J B P 1966 *Proc. R. Soc.* A **295** 300
[19] Johnson K L, Kendall K and Roberts A D 1971 *Proc. R. Soc.* A **324** 301
[20] Derjaguin B V, Muller V M and Toporov Y P 1975 *J. Colloid Interface Sci.* **53** 314
[21] Tabor D 1977 *J. Colloid Interface Sci.* **58** 2
[22] Maugis D 1992 *J. Colloid Interface Sci.* **150** 243
[23] Schwarz U D, Allers W, Gensterblum G and Wiesendanger R 1995 *Phys. Rev.* B **52** 14 976
[24] Meyer E, Overney R M, Howald L, Lüthi R, Frommer J and Güntherodt H-J 1992 *Phys. Rev. Lett.* **69** 1777
[25] Overney R M, Meyer E, Frommer J, Brodbeck D, Lüthi R, Howald L, Güntherodt H-J, Fujihira M, Takano H and Gotoh Y 1992 *Nature* **359** 133
[26] Scandella L, Meyer E, Howald L, Lüthi R, Guggisberg M, Gobrecht J and Güntherodt H-J 1996 *J. Vac. Sci. Technol.* B **14** 1255
[27] Teuschler T, Mahr K, Miyazaki S, Hundhausen M and Ley L 1995 *Appl. Phys. Lett.* **66** 2499
[28] Tamayo J, González L, González Y and García R 1996 *Appl. Phys. Lett.* **68** 2997
[29] Tamayo J, García R, Utzmeier T and Briones F 1997 *Phys. Rev.* B **55** R13 436
[30] Lüthi R, Haefke H, Meyer K-P, Meyer E and Howald L 1993 *J. Appl. Phys.* **74** 7461
[31] Eng L M, Friedrich M, Fousek J and Günter P 1996 *J. Vac. Sci. Technol.* B **14** 1191
[32] Bluhm H, Schwarz U D and Wiesendanger R 1998 *Phys. Rev.* B **57** 161
[33] Lüthi R, Haefke H, Meyer E, Howald L, Lang H-P, Gerth G and Güntherodt H-J 1994 *Z. Phys.* B **95**
[34] Lüthi R, Meyer E, Haefke H, Howald L, Gutmannsbauer W and Güntherodt H-J 1994 *Science* **266** 1979
[35] Bluhm H, Inoue T and Salmeron M 2000 *Phys. Rev.* B **61** 7760
[36] Schwarz U D, Zwörner O, Köster P and Wiesendanger R 1997 *Phys. Rev.* B **56** 6987
[37] Enachescu M, van der Oetelaar R J A, Carpick R W, Ogletree D F, Flipse C F J and Salmeron M 1998 *Phys. Rev. Lett.* **81** 1877
[38] Enachescu M, van den Oetelaar R J A, Carpick R W, Ogletree D F, Flipse C F J and Salmeron M 1999 *Tribol. Lett.* **7** 73
[39] Meyer E, Lüthi R, Howald L, Bammerlin M, Guggisberg M and Güntherodt H-J 1996 *J. Vac. Sci. Technol.* B **14** 1285
[40] Carpick R W, Agraït N, Ogletree D F and Salmeron M 1996 *J. Vac. Sci. Technol.* B **14** 1289
[41] Polaczyk C, Schneider T, Schöfer J and Santner E 1998 *Surf. Sci.* **402** 454
[42] Tabor D and Winterton R H S 1969 *Proc. R. Soc.* A **312** 435

[43] Israelachvili J N and Tabor D 1972 *Proc. R. Soc.* A **331** 19
[44] Johnson K L 1985 *Contact Mechanics* (Cambridge: Cambridge University Press)
[45] Carpick R W, Ogletree D F and Salmeron M 1997 *Appl. Phys. Lett.* **70** 1548
[46] Lantz M A, O'Shea S J, Welland M E and Johnson K L 1997 *Phys. Rev.* B **55** 10 776
[47] Lantz M A, O'Shea S J and Welland M E 1997 *Phys. Rev.* B **56** 15 345
[48] Sørensen M R, Jacobsen K W and Stoltze P 1996 *Phys. Rev.* B **53** 2101
[49] Zhong W and Tomànek D 1990 *Phys. Rev. Lett.* **64** 3054
[50] Gyalog T, Bammerlin M, Lüthi R, Meyer E and Thomas H 1995 *Europhys. Lett.* **31** 269
[51] Sasaki N, Kobayashi K and Tsukada M 1996 *Phys. Rev.* B **54** 2138
[52] Hölscher H, Schwarz U D and Wiesendanger R 1997 *Surf. Sci.* **375** 395
[53] Johnson K L and Woodhouse J 1998 *Tribol. Lett.* **5** 155
[54] Tománek D, Zhong W and Thomas H 1991 *Europhys. Lett.* **15** 887
[55] Gyalog T 1998 *PhD Thesis* University of Basel
[56] Pfeiffer O, Loppacher C, Wattinger C, Bammerlin M, Gysin U, Guggisberg M, Rast S, Bennewitz R, Meyer E and Güntherodt H-J 2000 *Appl. Surf. Sci.* **157** 337
[57] Landman U, Luedtke W D and Ribarsky M W 1989 *J. Vac. Sci. Technol.* A **7** 2829
[58] Landman U, Luedtke W D and Ringer E M 1992 *Wear* **153** 3
[59] Harrison J A, White C T, Colton R J and Brenner W 1992 *Surf. Sci.* **271** 57
[60] Shluger A L, Rohl A L, Wilson R M and Williams R T 1995 *J. Vac. Sci. Technol.* B **13** 1155
[61] Shluger A L, Rohl A L, Williams R T and Wilson R M 1995 *Phys. Rev.* B **52** 11 398
[62] Shluger A L, Williams R T and Rohl A L 1995 *Surf. Sci.* **343** 273
[63] Livshits A I and Shluger A L 1997 *Phys. Rev.* B **56** 12 482
[64] Ohzono T and Fujihira M 2000 *Phys. Rev.* B **62** 17 055
[65] Ohzono T and Fujihira M 2000 *Tribol. Lett.* **9** 63
[66] Buldum A and Ciraci S 1998 *Phys. Rev.* B **57** 2468
[67] Komanduri R, Chandrasekaran N and Raff L M 2000 *Phys. Rev.* B **61** 14 007
[68] Howald L, Meyer E, Lüthi R, Haefke H, Overney R, Rudin H and Güntherodt H-J 1993 *Appl. Phys. Lett.* **63** 117
[69] Howald L, Lüthi R, Meyer E, Gerth G, Haefke H, Overney R and Güntherodt H-J 1994 *J. Vac. Sci. Technol.* B **12** 2227
[70] Lüthi R, Meyer E, Haefke H, Howald L, Gutmannsbauer W, Guggisberg M, Bammerlin M and Güntherodt H-J 1995 *Surf. Sci.* **338** 247
[71] Lüthi R, Meyer E, Bammerlin M, Howald L, Haefke H, Lehmann T, Loppacher C, Güntherodt H-J, Gyalog T and Thomas H 1996 *J. Vac. Sci. Technol.* B **14** 1280
[72] Howald L, Lüthi R, Meyer E and Güntherodt H-J 1995 *Phys. Rev.* B **51** 5484
[73] Bennewitz R, Gyalog T, Guggisberg M, Bammerlin M, Meyer E and Güntherodt H-J 1999 *Phys. Rev.* B **60** R11 301
[74] Bennewitz R, Gnecco E, Gyalog T and Meyer E 2001 *Tribol. Lett.* **10** 51
[75] Germann G J, Cohen S R, Neubauer G, McClelland G M and Seki H 1993 *J. Appl. Phys.* **73** 163
[76] van den Oetelaar R J A and Flipse C F J 1997 *Surf. Sci.* **384** L828
[77] Fujisawa S, Kishi E, Sugawara Y and Morita S 1995 *Phys. Rev.* B **51** 7849
[78] Morita S, Fujisawa S and Sugawara Y 1996 *Surf. Sci. Rep.* **23** 3
[79] Kawakatsu H and Saito T 1996 *J. Vac. Sci. Technol.* B **14** 872
[80] Bouhacina T, Aimé J P, Gauthier S, Michel D and Heroguez V 1997 *Phys. Rev.* B **56** 7694
[81] Zwörner O, Hölscher H, Schwarz U D and Wiesendanger R 1998 *Appl. Phys.* A **66** S263
[82] Eyring H J 1937 *J. Chem. Phys.* **3** 107
[83] Glosli J N and McClelland G M 1993 *Phys. Rev. Lett.* **70** 1960
[84] Gourdon D *et al* 1997 *Tribol. Lett.* **3** 317
[85] Hirano M, Shinjo K, Kaneko R and Murata Y 1991 *Phys. Rev. Lett.* **67** 2642
[86] Overney R M, Takano H, Fujihira M, Paulus W and Ringsdorf H 1994 *Phys. Rev. Lett.* **72** 3546
[87] Takano H and Fujihira M 1996 *J. Vac. Sci. Technol.* B **14** 1272
[88] Liley M, Gourdon D, Stamou D, Meseth U, Fischer T M, Lautz C, Stahlberg H, Vogel H, Burnham N A and Duschl C 1998 *Science* **280** 273
[89] Sheehan P E and Lieber C M 1996 *Science* **272** 1158
[90] Falvo M R, Taylor R M, Helser A, Chi V, Brooks F P Jr, Wahburn S and Superfine R 1999 *Nature* **397** 236
[91] Falvo M R, Steele J, Taylor R M II and Superfine R 2000 *Tribol. Lett.* **9** 73
[92] Weisenhorn A L, Maivald P, Butt H-J and Hansma P K 1992 *Phys. Rev.* B **45** 11 226
[93] Binggeli M and Mate C M 1994 *Appl. Phys. Lett.* **65** 415

[94] Hu J, Xiao X D, Ogletree D F and Salmeron M 1995 *Surf. Sci.* **327** 358
[95] Putman C A J, Igarshi M and Kaneko R 1995 *Appl. Phys. Lett.* **66** 3221
[96] Schumacher A, Kruse N, Prins R, Meyer E, Lüthi R, Howald L, Güntherodt H-J and Scandella L 1996 *J. Vac. Sci. Technol.* B **14** 1264
[97] Xu L, Bluhm H and Salmeron M 1998 *Surf. Sci.* **407** 251
[98] Marti A, Hähner G and Spencer N D 1995 *Langmuir* **11** 4632
[99] Persson B N J 1991 *Phys. Rev.* B **44** 3277
[100] Krim J, Solina D H and Chiarello R 1991 *Phys. Rev. Lett.* **66** 181
[101] Mak C, Daly C and Krim J 1994 *Thin Solid Films* **253** 190
[102] Dayo A, Alnasrallah W and Krim J 1998 *Phys. Rev. Lett.* **80** 1690
[103] Persson B N J, Tosatti E, Fuhrmann D, Witte G and Wöll Ch 1999 *Phys. Rev.* B **59** 11 777
[104] Merrill P B and Perry S S 1998 *Surf. Sci.* **418** 342
[105] Frisbie C D, Rozsnyai L F, Noy A, Wrighton M S and Lieber C M 1994 *Science* **265** 2071
[106] Ito T, Namba M, Buhlmann P and Umezawa Y 1997 *Langmuir* **13** 4323
[107] Tsukruk V V and Bliznyuk V N 1998 *Langmuir* **14** 446
[108] Ando Y and Ino J 1998 *Wear* **216** 115
[109] Ando Y, Nagashima T and Kakuta K 2000 *Tribol. Lett.* **9** 15
[110] Heim L-O, Blum J, Preuss M and Butt H-J 1999 *Phys. Rev. Lett.* **83** 3328